ChemComm

Accepted Manuscript

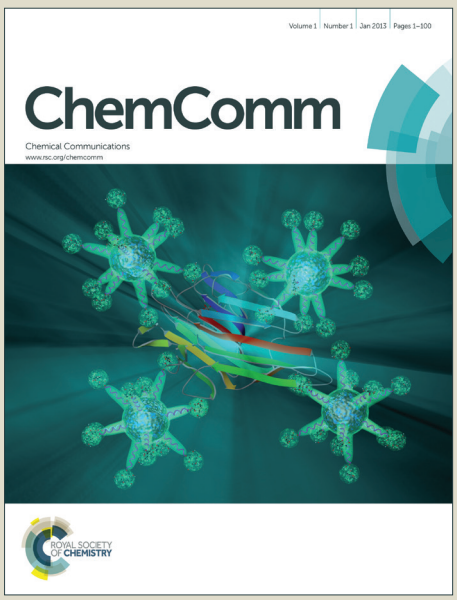

ROYAL SOCIETY OF CHEMISTRY

www.rsc.org/chemcomm

ChemComm

RSCPublishing

COMMUNICATION

Free energy calculations of A_{2A} adenosine receptor mutation effects on agonist binding

Cite this: DOI: 10.1039/x0xx00000x

Henrik Keränen[a], Johan Åqvist[a] and Hugo Gutiérrez-de-Terán*[a]

Received 00th January 2012,
Accepted 00th January 2012

DOI: 10.1039/x0xx00000x

www.rsc.org/

A general computational scheme to evaluate the effects of single point mutations on ligand binding is reported. This scheme is applied to characterize agonist binding to the A_{2A} adenosine receptor, and is found to accurately explain how point mutations of different nature affect the binding affinity of a potent agonist.

One of the major experimental approaches to characterize G-protein coupled receptors (GPCRs) is site-directed mutagenesis. In combination with experimental or modelled 3D structures, it provides an important information resource for understanding receptor function and ligand binding properties.[1] A good example is the A_{2A} adenosine receptor (A_{2A}AR). This is one of the most widely characterized GPCRs with several high resolution crystal structures for both inactive[2-6] and active-like[7,8] receptors (denoted A_{2A}AR* herein), and extensive mutagenesis data available.[9-14] This has allowed conformational characterization of the receptor and ligand design by computational approaches.[15-20] A number of A_{2A}AR mutants have been characterized via radioligand binding. Binding affinities of different compounds can then be measured by competition assays, resulting in ligand affinity ratios between mutant and wt receptor (K_i^{mut}/K_i^{wt}).[10-14]

Computation of such ligand affinity ratios is in principle possible through free energy perturbation (FEP) simulations, sometimes referred to as "computational alchemy". However, convergence and sampling problems associated with the method appear to have limited the number of such applications. We have recently introduced an efficient calculation scheme to evaluate the effect of alanine mutations on ligand binding,[21] which allowed us to explain both agonist and antagonist binding properties of 18 different mutants of A_{2A}AR.[22] The given sidechain is mutated to alanine in two parallel molecular dynamics (MD) simulations, with and without the ligand bound to the receptor site. The binding free energy difference between wt and mutant receptor can then be calculated via a standard thermodynamic cycle (left cycle of Fig. 1). The convergence problem associated with large perturbations, such as Trp→Ala, is solved by dividing the given mutation into a series of smaller subperturbations, thereby creating a smoother transformation between the end-states.[21] Each subperturbation is also divided into a relatively large number of FEP windows (~50 λ-steps), where every window is sampled for 10-40 ps. The subperturbations correspond to groups of atoms being successively annihilated, based on their topological distance to the protein backbone. During annihilation of a residue each atom group will undergo three consecutive transformations *i*) annihilation of partial charges, *ii*) transformation of regular van der Waals (Lennard-Jones) potential to a soft-core potential to prevent singularities,[23] and *iii*) annihilation of the soft-core potential.

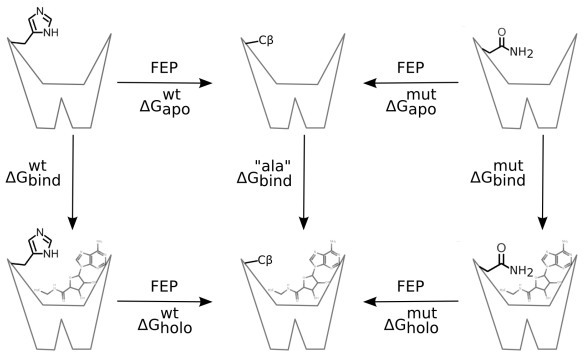

Fig. 1 Thermodynamic cycle for a His → Asn mutation. The two thermodynamic cycles of His → Ala (left cycle) and Asn → Ala (right cycle) are shown. By mutating the two (wt and mutant) end-state sidechains to a common intermediate (bare Cβ) state, the two cycles can be connected and the relative binding free energy between mutant and wt calculated.

We now generalize the above FEP scheme to be able to deal with any amino acid mutation. This is done by joining two thermodynamic cycles describing the reduction of a sidechain, for wt and mutant, to a common fragment. For practical purposes, this is chosen as a bare Cβ carbon and thus approximates an alanine sidechain (Fig. 1). The resulting double thermodynamic cycle yields the change in binding free energy due to a mutation as

$$\Delta\Delta G_{bind}^{mut-wt} = \left(\Delta G_{holo}^{wt} - \Delta G_{apo}^{wt}\right) - \left(\Delta G_{holo}^{mut} - \Delta G_{apo}^{mut}\right)$$

Here, one performs a total of four independent simulations to account for each mutation: wt → Cβ and mutant → Cβ, each in both holo and apo states. When performing several mutations for the

same position, the wt "legs" of the cycle only need to be calculated once and can be reused for any mutation at that position. This way, by combining 19 MD simulations accounting for each possible R → Cβ annihilation (R = any sidechain), one could estimate the effect of all possible 20x19/2=190 mutations. This FEP/MD scheme is used herein to analyse the effects on A_{2A}AR*-NECA binding of 17 mutations, at eight different positions, which have been reviewed by Martinelli and Tuccinardi[24] (Fig. 2, Table S1, ESI†).

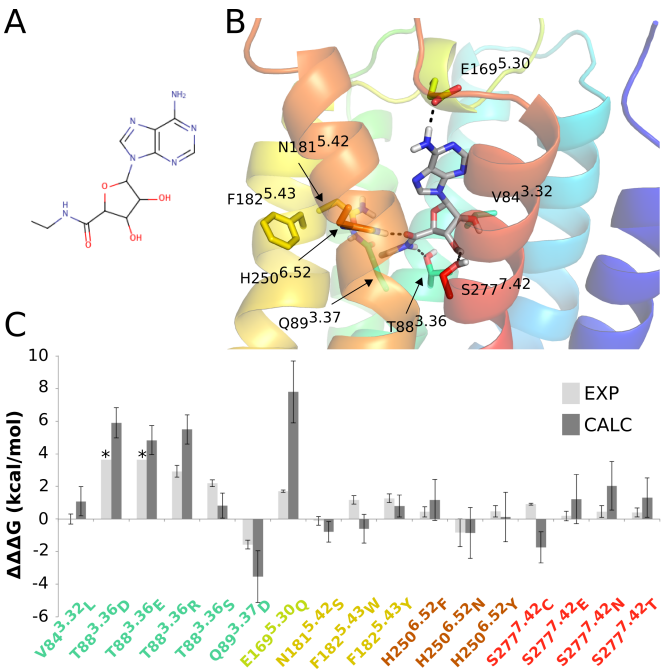

Fig. 2 Structure of (A) the agonist NECA and (B) the wt-A_{2A}AR*-NECA complex used for the simulations. Transmembrane helices are rainbow-coloured from the N terminal (TM1-blue) to C terminal (TM7-red). Mutated residues mutated are shown as sticks and hydrogen bonds as dashed lines. (C) Calculated (dark grey) and experimental (light grey) NECA binding free energy differences between each A_{2A}AR* mutant and the wt receptor. The star symbol in the plot denotes that an experimental value could not be determined and represents the detection threshold in the experiment.

The initial A_{2A}AR*-NECA complex was obtained by combining structural information from A_{2A}AR crystal structures (see ESI† and Ref. [25] for details). The receptor complex was embedded in a lipid bilayer, solvated, and equilibrated using GROMACS4.0.5[26] with the protocol implemented in the GPCR-ModSim web-server.[27] For subsequent simulations of the binding site region, a 25 Å radius sphere centred on NECA was extracted from the equilibrated system. The spherical system was used for MD simulations with the program Q[28] and the OPLS all-atom (OPLS-AA) force field[29,30] (see ESI† for details of the MD simulation and FEP analysis). The use of reduced spherical models restricts the sampling to the area of interest and therefore accelerates convergence, as compared to the commonly used periodic boundary models. Initial models of mutant receptors were created by modelling the structurally most probable rotamer of the mutated residue. If more than one rotamer could be modelled, all were subjected to MD simulation. In the few cases were these rotamers did not converge to the same structure, each of them were subjected to mutation calculations (see ESI†).

Our predicted binding free energies show good agreement with experimental data, demonstrating the capacity of the FEP scheme to discriminate mutations that cause large effects from those with negligible (or even favourable) contributions to ligand binding (Fig. 2 and Table S1, ESI†). This is particularly remarkable considering the wide spectrum of mutations evaluated. The precision of the results is evaluated from the set of independent replicate simulations, yielding an overall average standard error of mean (s.e.m.) of 1.2 kcal/mol. Naturally, the statistical errors in the calculations are expected to increase by a factor of $\sqrt{2}$ as compared to alanine mutations, since two independent sets of transformations (wt → Cβ and mutant → Cβ) have to be carried out in the present case for both the holo and apo states (see ESI†). This is precisely what we observe, as the average precision for the corresponding alanine mutations was 0.7 kcal/mol.[22] The convergence of the simulations is assessed by calculating the hysteresis, i.e. the difference of applying the FEP formula in forward and reverse direction for each individual simulation. Here, the average hysteresis is 0.3 kcal/mol, which is equally low as for the alanine mutations performed on the same system.[22]

A few mutations are worth examining in more detail, since they illustrate the power of the simulations for predicting the structural origins of changes in ligand binding affinity. Among these, Q89$^{3.37}$D is particularly intriguing since the buried location of this position in a hydrophobic environment is suggestive of a protonated (neutral) aspartic acid. Consequently, calculations were performed for both protonation states of the mutant, yielding $\Delta\Delta G_{bind} = 9.6\pm1.5$ kcal/mol for unprotonated and $\Delta\Delta G_{bind} = -3.5\pm1.6$ kcal/mol for protonated state of the residue. The latter value is in agreement with the experimental data and shows that the protonated aspartic acid favours binding of NECA. This is further supported by the pK_a predicted for this sidechain using Propka,[31] which indicates a pK_a value above physiological pH. This criterion, together with a close examination of the H-bond network, should be used to decide the most probable protonation state. Similarly, both the T88$^{3.36}$D and T88$^{3.36}$E mutants are predicted to be in their neutral form (Table S1, ESI†). Thus, while an important feature of the present simulation scheme is to be able to perform mutations in an automated manner, changes in protonation states represent another level of complexity that needs careful consideration.

The above problem also pertains to E169$^{5.30}$ in EL2, which makes a salt bridge with H264^{ECL3} and also a direct hydrogen bond to the exocyclic amine group of NECA. The large effect observed for alanine mutation at this position[9] was captured in our earlier work,[22] where the histidine was maintained in its charged state. However, a solvent-exposed histidine has a pK_a of ~6.5, indicating that it would be deprotonated in absence of any counter-ion. Hence, to describe the E169$^{5.30}$A mutant properly, it is likely that H264^{ECL3} should become deprotonated when E169$^{5.30}$ is mutated to alanine. Likewise, for the E169$^{5.30}$Q mutation the optimal starting point for the Q169$^{5.30}$ state may also be an unprotonated H264^{ECL3}. To examine this possibility, we performed two sets of additional calculations. These show that the E169$^{5.30}$A mutant is not sensitive to the protonation state of the histidine (Table S2, ESI†). The E169$^{5.30}$Q mutation, however, shows distinctly better agreement with experiment with neutral histidine (Table S1, ESI†), confirming the hypothesis that H264^{ECL3} becomes deprotonated upon E169$^{5.30}$Q/A mutations. Another interesting case is H250$^{6.52}$, responsible for stabilization of the carboxamide moiety in NECA through a hydrogen bond. Mutation to a non-polar and aromatic residue (H250$^{6.52}$F) has a negative impact on NECA affinity. Recovery of polarity restores wt ligand binding affinity, as demonstrated by H250$^{6.52}$N, which is predicted to maintain the hydrogen bond network (Fig. 3) and even has a slightly higher binding affinity than wt (Fig. 2). Further, the H250$^{6.52}$Y mutant essentially behaves as H250$^{6.52}$F, indicating that the aromatic hydroxyl group has a negligible contribution. Encouragingly, all these effects are accurately reproduced and explained by the simulations (Fig. 2 and Table S1, ESI†).

As mentioned earlier, mutations corresponding to the left side of the thermodynamic cycle (Fig. 1) can be correlated to alanine-scanning data for the given position. Indeed, a near perfect correlation (r^2 = 0.99, Table S2, ESI†) is obtained between bare Cβ ($\Delta\Delta G_{C\beta}^{FEP}$) and alanine ($\Delta\Delta G_{Ala}^{FEP}$) mutations for five out of the six positions considered both here and in our earlier work.[22] The S277$^{7.42}$A mutation, however, stands out with $\Delta\Delta G_{Ala}^{FEP} - \Delta\Delta G_{C\beta}^{FEP} =$ 1.7 kcal/mol. In this case, the present simulations, which do not end up with a true alanine sidechain methyl group, consistently allow a water molecule to enter and replace the interaction of the wt serine. As this did not occur for the earlier S277$^{7.42}$A mutation,[22] it appears that the missing hydrogen repulsive Lennard-Jones potentials in pseudo-alanine state are, in fact, important for defining the cavity volume accessible to water. The only mutant in this position where a water molecule was not let in was the Cys→Cβ transformation. This led to a somewhat different intermediate state as compared to the wt mutation, which could explain the discrepancy between calculated and experimental values (Fig. 2).

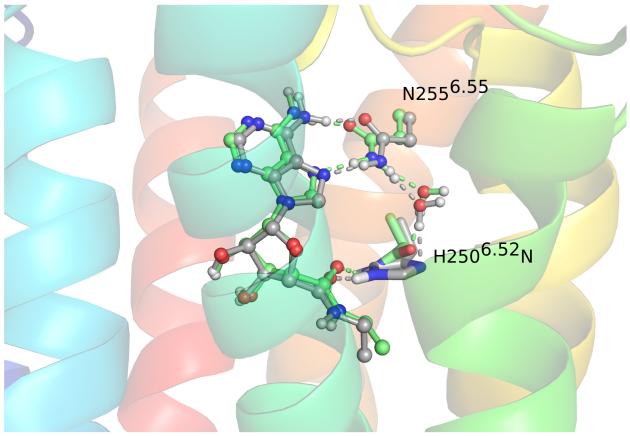

Fig. 3 Conserved interactions for the H250$^{6.52}$N mutation in agonist binding. The average MD conformation of the A_{2A}AR*-NECA H250$^{6.52}$N mutant complex (green) with interacting sidechains and water molecules is shown, overlaid on the wt average MD conformation (grey). The H/N250$^{6.52}$ sidechains are shown as sticks, conserved interaction networks in dashed lines, the ligand in ball-and-stick, and helices as cartoons (TM1 - blue → TM7 - red).

Computational methods for accurate predictions of structural and energetic effects of point mutations on ligand binding are of considerable interest in biochemistry and pharmacology. This is particularly true for GPCRs and motivated our development of an accurate and efficient method to computationally predict and analyse experimental alanine-scanning data.[21,22] In the present work, the computational alanine-scanning method is extended to be able to accurately obtain relative ligand binding free energies for arbitrary mutations of a receptor protein. Even though this method involves the evaluation of a double thermodynamic cycle, good precision is retained (~1 kcal/mol) with total MD simulation times on the order of 60-120 ns (see ESI†).

It should be noted that alternative approaches could in principle be considered for computational mutagenesis, but may be subject to limitations. For example, with the standard single-topology FEP technique[32,33] a seemingly simple mutation from tyrosine to histidine (6-membered to 5-membered ring) is actually rather complicated to carry out. This is because the covalent bonding of the sidechain changes substantially and is difficult to treat efficiently with the usual dummy atom approach.[34] An alternative here is to use the so-called dual-topology method[35,36] which has a mixture of both sidechains present simultaneously during simulations, the weights of the two states (sidechains) being successively varied along the transformation path. In that case the entire sidechain of one state is usually annihilated in a single calculation, while the target sidechain is concomitantly created. However, treating only annihilation of sidechains has clear advantages compared to the alternative of "growing" a larger sidechain out of a smaller one in the calculations. This is because the conformation of the mutant residue can be optimized and, e.g., different rotamers can be systematically tested and selected based on structural and energetic criteria. In the case where larger sidechains are created (or grown) out of smaller ones there is essentially no control over the final conformation. In addition, convergence is usually better when the number of degrees of freedom of the system is reduced (atom annihilation) rather than increased (atom creation).

The point above can be illustrated here with the H250$^{6.52}$N mutant, which retains similar polar interactions in wt and mutant receptors. When instead growing both the wt and mutant sidechains from the common Cβ starting point, the resulting NECA binding free energy difference is in stark disagreement with experiment and the precision of the calculations is also completely lost (Table 1). The reason for this is that there is no control of the final sidechain conformations, which essentially become randomized among the different simulation replicas. In this example, the hydrogen bond network (Fig. 3) is not attained in either of the wt or mutant states, as opposed to the double annihilation scheme where the initial structures of both wt and mutant receptors can be confidently modelled.

Table 1. Comparison between alternative mutagenesis protocols for selected mutations and experimental NECA relative binding free energies for A_{2A}AR mutants (kcal/mol).[a]

Position	$\Delta\Delta G_{bind}^{alternative}$	$\Delta\Delta G_{bind}^{default}$[d]	$\Delta\Delta G_{bind}^{exp}$
H250$^{6.52}$N	3.5 ± 4.3[b]	-0.9 ± 1.6	-0.8 ± 0.9
V84$^{3.32}$L	-0.2 ± 0.9[c]	1.1 ± 0.9	0.0 ± 0.3
F182$^{5.42}$Y	0.3 ± 0.2[c]	0.8 ± 0.7	1.3 ± 0.3

[a] Experimental relative binding free energies ($\Delta\Delta G_{bind}^{exp}$) calculated from K_i values as $\Delta\Delta G_{bind}^{exp} = RTln(K_i^{mut}/K_i^{wt})$. [b] Growth of sidechains instead of annihilation. [c] Annihilation of sidechains until the first common intermediate state. [d] The protocol described in this work.

Another interesting, but slightly more complex, alternative for increasing the precision of the calculations would be to devise a specific optimal common intermediate for each possible pair of wt and mutant amino acids. At a first glance, it may seem that this would involve 20×19/2=190 different recipes for all possible amino acid mutations. This is, however, not the case if we adhere to the main principle of our method,[21,22] which is to not touch any bonded terms in the transformations involved in the free energy calculations. That is, the good convergence of the method is largely due to the choice of smoothly annealing atoms rather than to change, e.g., bond lengths and angles, which can cause large fluctuations of the energy gap between the states involved in the free energy calculation. Hence, if one would carry out a mutation from aspartic acid to leucine or asparagine, where all three sidechains have the same basic topology, the choice would still be to go to alanine in order not to have to change any bonded terms. Based on this principle one can estimate that there will be fewer than ten distinct recipes involved in order to cover all possible mutations. On the other hand, for a Leu to Ile mutation the largest common fragment that does not involve changing bonded terms would correspond to retaining Cγ and thus not going all the way to alanine. Likewise, mutations involving flexible sidechains such as transformations between Lys, Met, Arg, Glu, Gln, Leu or Ile, could in principle retain Cδ in the common fragment. However, the flexibility of these sidechains might cause

the common fragment to end up in different stable conformations. If so, the intermediate state joining the two thermodynamic cycles (Fig 1) would not be unique, and proceeding further to Cβ could solve the problem. Whether such alternative FEP "shortcuts" would offer an improvement is thus not guaranteed and it is difficult to generalize the effects on robustness and precision.

Among the mutations evaluated here, two mutants are suitable for evaluating this alternative approach, namely V84$^{3.32}$L and F182$^{5.42}$Y. In the first case the common fragment retains the Cγ atom, which gives a slightly better prediction of the experimental result but with the same calculation precision as the default protocol (Table 1) For the phenylalanine to tyrosine mutation the largest common fragment retains the bare Cζ carbon. The calculations for F182$^{5.42}$Y with this approach, as expected, yield a better precision due to fewer subperturbations but the prediction is not improved (Table 1). Hence, while optimization of this type of alternative approach may deserve further study, an advantage with our main scheme is that the calculation for the wt mutation to alanine can be reused for any mutation at the given position.

The prospect of being able to routinely carry out reliable computational predictions of effects of mutations on ligand binding is very attractive. It would be useful not only for characterization of ligand selectivities in complex signalling systems such as GPCRs, but perhaps most importantly for addressing problems of drug resistance in pathogens as well as individual responses to drug treatment due to genetic variation. In this respect, it is somewhat surprising that the free energy perturbation type of methodology, which has been around for almost 30 years, has not yet really become common practice in addressing these problems. This is most likely due to the fact that the method is well-known to converge better the smaller the perturbations involved are, which has arguably led to a focus on calculations of smaller chemical substitutions on ligand molecules. However, as shown here, the step towards treating mutations between arbitrary amino acids is not that great in view of the fact that their chemical repertoire is limited and that efficient protocols can indeed be developed.

Support from the Swedish Research Council (VR grant 521-2014-2118), the eSSENCE e-science initiative and the Swedish National Infrastructure for Computing (SNIC) are gratefully acknowledged.

Notes and references

[a] *Department of Cell and Molecular Biology, Uppsala University, Biomedical Center, Box 596, SE-751 24 Uppsala, Sweden. Email: hugo.gutierrez@icm.uu.se*

† Electronic Supplementary Information (ESI) available: Full description of computational methods. Calculated and experimental NECA relative binding free energies for A_{2A}AR mutants, including values for each subperturbation (Table S1) and comparison between Cβ and alanine mutations (Table S2). See DOI: 10.1039/c000000x/

1. J. A. Salon, J. A. Salon, D. T. Lodowski, D. T. Lodowski, K. Palczewski, and K. Palczewski, *Pharmacol. Rev.*, 2011, **63**, 901–937.
2. V.-P. Jaakola, M. T. Griffith, M. A. Hanson, V. Cherezov, E. Y. T. Chien, J. R. Lane, A. P. IJzerman, and R. C. Stevens, *Science*, 2008, **322**, 1211–1217.
3. A. S. Doré, N. Robertson, J. C. Errey, I. Ng, K. Hollenstein, Ben Tehan, E. Hurrell, K. Bennett, M. Congreve, F. Magnani, C. G. Tate, M. Weir, and F. H. Marshall, *Structure/Folding and Design*, 2011, **19**, 1283–1293.
4. M. Congreve, S. P. Andrews, A. S. Doré, K. Hollenstein, E. Hurrell, C. J. Langmead, J. S. Mason, I. W. Ng, B. Tehan, A. Zhukov, M. Weir, and F. H. Marshall, *J. Med. Chem.*, 2012, **55**, 1898–1903.
5. T. Hino, T. Arakawa, H. Iwanari, T. Yurugi-Kobayashi, C. Ikeda-Suno, Y. Nakada-Nakura, O. Kusano-Arai, S. Weyand, T. Shimamura, N. Nomura, A. D. Cameron, T. Kobayashi, T. Hamakubo, S. Iwata, and T. Murata, *Nature*, 2012, **482**, 237–240.
6. W. Liu, E. Chun, A. A. Thompson, P. Chubukov, F. Xu, V. Katritch, G. W. Han, C. B. Roth, L. H. Heitman, A. P. IJzerman, V. Cherezov, and R. C. Stevens, *Science*, 2012, **337**, 232–236.
7. G. Lebon, T. Warne, P. C. Edwards, K. Bennett, C. J. Langmead, A. G. W. Leslie, and C. G. Tate, *Nature*, 2011, **474**, 521–525.
8. F. Xu, H. Wu, V. Katritch, G. W. Han, K. A. Jacobson, Z. G. Gao, V. Cherezov, and R. C. Stevens, *Science*, 2011, **332**, 322–327.
9. J. Kim, Q. Jiang, M. Glashofer, S. Yehle, J. Wess, and K. A. Jacobson, *Molecular Pharmacology*, 1996, **49**, 683–691.
10. Q. Jiang, A. M. van Rhee, J. Kim, S. Yehle, J. Wess, and K. A. Jacobson, *Molecular Pharmacology*, 1996, **50**, 512–521.
11. J. Kim, J. Wess, A. M. van Rhee, T. Schöneberg, and K. A. Jacobson, *J. Biol. Chem.*, 1995, **270**, 13987–13997.
12. Q. Jiang, B. X. Lee, M. Glashofer, A. M. van Rhee, and K. A. Jacobson, *J. Med. Chem.*, 1997, **40**, 2588–2595.
13. Z.-G. Gao, Q. Jiang, K. A. Jacobson, and A. P. IJzerman, *Biochemical Pharmacology*, 2000, **60**, 661–668.
14. S.-K. Kim, Z.-G. Gao, P. Van Rompaey, A. S. Gross, A. Chen, S. Van Calenbergh, and K. A. Jacobson, *J. Med. Chem.*, 2003, **46**, 4847–4859.
15. D. Rodríguez, A. Piñeiro, and H. Gutiérrez-de-Terán, *Biochemistry*, 2011, **50**, 4194–4208.
16. J. Carlsson, L. Yoo, Z.-G. Gao, J. J. Irwin, B. K. Shoichet, K. A. Jacobson, and K. A. Jacobson, *J. Med. Chem.*, 2010, **53**, 3748–3755.
17. V. Katritch, V.-P. Jaakola, J. R. Lane, J. Lin, A. P. IJzerman, M. Yeager, I. Kufareva, R. C. Stevens, and R. Abagyan, *J. Med. Chem.*, 2010, **53**, 1799–1809.
18. E. van der Horst, R. van der Pijl, T. Mulder-Krieger, A. Bender, A. P. IJzerman, and A. P. IJzerman, *ChemMedChem*, 2011, **6**, 2302–2311.
19. C. J. Langmead, S. P. Andrews, M. Congreve, J. C. Errey, E. Hurrell, F. H. Marshall, J. S. Mason, C. M. Richardson, N. Robertson, A. Zhukov, and M. Weir, *J. Med. Chem.*, 2012, **55**, 1904–1909.
20. D. K. Tosh, K. Phan, Z.-G. Gao, A. A. Gakh, F. Xu, F. Deflorian, R. Abagyan, R. C. Stevens, K. A. Jacobson, and V. Katritch, *J. Med. Chem.*, 2012, **55**, 4297–4308.
21. L. Boukharta, H. Gutiérrez-de-Terán, and J. Åqvist, *PLoS Comput. Biol.*, 2014, **10**, e1003585.
22. H. Keränen, H. Gutiérrez-de-Terán, and J. Åqvist, *PLoS ONE*, 2014, **9**, e108492.
23. T. C. Beutler, A. E. Mark, R. C. van Schaik, P. R. Gerber, and W. F. van Gunsteren, *Chem. Phys. Lett.*, 1994, **222**, 529–539.
24. A. Martinelli and T. Tuccinardi, *Med. Res. Rev.*, 2008, **28**, 247–277.
25. H. Gutiérrez-de-Terán, A. Massink, D. Rodríguez, W. Liu, G. W. Han, J. S. Joseph, I. Katritch, L. H. Heitman, L. Xia, A. P. IJzerman, V. Cherezov, V. Katritch, and R. C. Stevens, *Structure/Folding and Design*, 2013, **21**, 2175–2185.
26. B. Hess, C. Kutzner, D. van der Spoel, E. Lindahl, and E. Lindahl, *J. Chem. Theory Comput.*, 2008, **4**, 435–447.
27. H. Gutiérrez-de-Terán, X. Bello, and D. Rodríguez, *Biochem. Soc. Trans.*, 2013, **41**, 205–212.
28. J. Marelius, K. Kolmodin, I. Feierberg, and J. Aqvist, *J. Mol. Graph. Model.*, 1998, **16**, 213–225.
29. W. L. Jorgensen, D. S. Maxwell, J. Tirado-Rives, and J. Tirado-Rives, *J. Am. Chem. Soc.*, 1996, **118**, 11225–11236.
30. G. A. Kaminski, R. A. Friesner, J. Tirado-Rives, and W. L. Jorgensen, *J. Phys. Chem. B*, 2001, **105**, 6474–6487.
31. M. H. M. Olsson, C. R. Søndergaard, M. Rostkowski, and J. H. Jensen, *J. Chem. Theory Comput.*, 2011, **7**, 525–537.
32. W. L. Jorgensen and C. Ravimohan, *J. Chem. Phys.*, 1985, **83**, 3050.
33. D. A. Pearlman, *J. Phys. Chem.*, 1994, **98**, 1487–1493.
34. B. O. Brandsdal, F. Osterberg, M. Almlöf, I. Feierberg, V. B. Luzhkov, J. Åqvist, and J. Åqvist, *Adv. Protein Chem.*, 2003, **66**, 123–158.
35. J. Gao, K. Kuczera, B. Tidor, and M. Karplus, *Science*, 1989, **244**, 1069–1072.
36. S. Boresch and M. Karplus, *J. Phys. Chem. A*, 1999, **103**, 103–118.

